Experimental and Detailed Modeling Study of the Effect of Water Vapor on the Kinetics of Combustion of Hydrogen and Natural Gas, Impact on NO$_x$

T. Le Cong and P. Dagaut*

Centre National de la Recherche Scientifique 1C, Avenue de la Recherche Scientifique − 45071 Orléans Cedex 2, France

The dilution of fuel−air mixtures by exhaust gases (mainly CO_2, H_2O, and CO) affects the kinetics of combustion. This dilution is used in gas turbines and flameless combustor to reduce pollutant emissions, particularly nitrogen oxides (NO$_x$). Therefore, studying the effect of these compounds on the kinetics of oxidation of fuels such as natural gas and hydrogen is needed. The oxidation of H_2 and that of CH_4 were studied experimentally in a fused silica jet-stirred reactor (JSR) from fuel-lean to fuel-rich conditions, over the temperature range 800−1300 K. The experiments were repeated in the presence of 10% in mol of H_2O. A detailed chemical kinetic modeling of these experiments and of literature data (ignition delays, flame speed) was performed using a detailed kinetic reaction mechanism. Good agreement between the data and this modeling was obtained. Sensitivity and reaction paths analyses were used to respectively delineate the influencing and important reactions for the kinetics of oxidation of the fuels in the presence of H_2O. The proposed kinetic reaction mechanism helps us to understand the inhibiting effect of water vapor on the oxidation of hydrogen and methane. The effect of H_2O on NO$_x$ formation under gas turbine conditions was also investigated numerically, showing the reduction of NO$_x$ emissions is mainly due to dilution and thermal effects.

1. Introduction

Flameless combustion is an emerging combustion concept that can be useful for reducing pollutant emissions, particularly NO$_x$, and improve combustion efficiency.[1] There, the reactants are preheated and diluted by exhaust gases, mainly CO, CO_2, and H_2O, and traces of NO$_x$. Also, in gas turbines, water vapor is also injected to limit NO$_x$ formation.[2−4] Thus, it is important to study the effect of such compounds on the kinetics of oxidation of conventional and nonconventional fuels. The effect

of NO$_x$ and CO_2 recirculation was previously addressed,[5−8] whereas that of water vapor was not.

In this Article, we present new experimental results obtained for the neat oxidation of hydrogen and methane in a JSR at 1 atm, over a wide range of equivalence ratio ($\varphi = 0.1-1.5$), for temperatures in the range 800−1300 K and constant mean residence time (τ). Corresponding experiments where 10% H_2O (in mol) is present in the reacting mixtures were performed. The oxidation of these fuels under JSR, shock-tube, and premixed flame conditions was modeled. The reduction of NO$_x$ formation in the presence of water vapor was also computationally investigated. Kinetic analyses including sensitivity analyses and reaction path analyses were used to rationalize the results.

2. Experimental Section

We used the experimental setup presented earlier.[9−11] The JSR consisted of a small sphere of 4 cm o.d. (30 cm^3) made of fused-silica (to minimize wall catalytic reactions), equipped with 4 nozzles of 1 mm i.d. for the admission of the gases, which are achieving the stirring. A nitrogen flow of 100 L/h was used to dilute the fuel. As before,[9−11] all of the gases were preheated before injection to minimize temperature gradients inside the reactor. The flow rates were measured and regulated by thermal mass-flow controllers. The

* To whom correspondence should be addressed. Telephone: (33) 238 25 54 66. E-mail: dagaut@cnrs-orleans.fr.

(1) Cavaliere, A.; de Joannon, M. Mild combustion. *Prog. Energy Combust. Sci.* **2004,** *30,* 329–366.

(2) Skevis, G.; Chrissanthopoulos, A.; Goussis, D. A.; Mastorakos, E.; Derksen, M. A. F.; Kok, J. B. W. Numerical investigation of methane combustion unde mixed air-steam gas turbine conditions−FLAMESEEK. *Appl. Therm. Eng.* **2004,** *24,* 1607–1618.

(3) De Jager, B.; Kok, J. B. W.; Skevis, G. Effect of water addition on polluant formation from LPP gas turbine combustors. *Proc. Combust. Inst.* **2007,** *31,* 3123–3130.

(4) Jonsson, M.; Yan, J. Humidified gas turbines−a review of proposed and implemented cycles. *Energy* **2005,** *30,* 1013–1078.

(5) Dagaut, P.; Nicolle, A. Experimental and detailed kinetic modeling study of the effect of exhaust gas on fuel combustion: Mutual sensitization of the oxidation of nitric oxide and methane over extended temperature and pressure ranges. *Combust. Flame* **2005,** *140,* 161–171.

(6) Dagaut, P.; Mathieu, O.; Nicolle, A.; Dayma, G. Experimental and detailed kinetic modeling study of the mutual sensitization of the oxidation of nitric oxide, ethane and ethylene. *Combust. Sci. Technol.* **2005,** *177,* 1767–1791.

(7) Nicolle, A.; Dagaut, P. Occurrence of NO-reburning in MILD combustion evidenced via chemical kinetic modeling. *Fuel* **2006,** *85,* 2469–2478.

(8) Le Cong, T.; Dagaut, P.; Dayma, G. Oxidation of natural gas, natural gas/syngas mixtures and effect of burnt gas recirculation: Experimental and detailed kinetic modeling. *J. Eng. Gas Turbines Power* **2008,** *130,* 041502-1,10.

(9) Dagaut, P. On the kinetics of hydrocarbons oxidation from natural gas to kerosene and diesel fuel. *Phys. Chem. Chem. Phys.* **2002,** *4,* 2079–2094.

(10) Tan, Y.; Dagaut, P.; Cathonnet, M.; Boettner, J.-C. Acetylene oxidation in a JSR from 1 to 10 atm and comprehensive kinetic modeling. *Combust. Sci. Technol.* **1994,** *102,* 21–55.

(11) Dagaut, P.; Cathonnet, M.; Rouan, J. P.; Foulatier, R.; Quilgars, A.; Boettner, J. C.; Gaillard, F.; James, H. A jet stirred reactor for kinetic studies of homogeneous gas phase reactions at pressure above one atmosphere. *J. Phys. E: Instrum.* **1986,** *19,* 207–209.
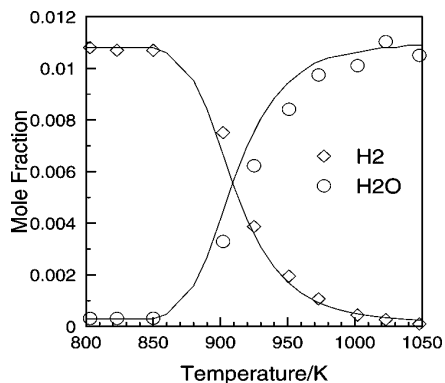
Figure 1. The oxidation of hydrogen$-N_2-O_2$ in a JSR (1 atm, $\tau = 120$ ms, 1% H_2, $\varphi = 0.2$, dilution by nitrogen). The data (large symbols) are compared to the modeling (lines).
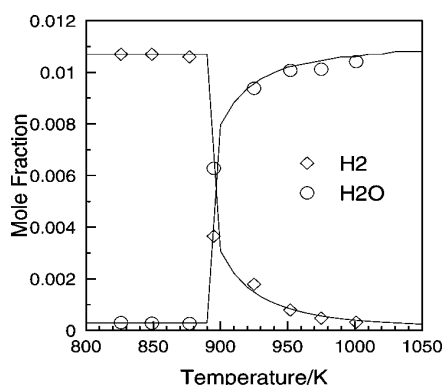

Figure 2. The oxidation of hydrogen$-N_2-O_2$ in a JSR (1 atm, $\tau = 120$ ms, 1% H_2, $\varphi = 0.5$, dilution by nitrogen). The data (large symbols) are compared to the modeling (lines).

Figure 3. The oxidation of hydrogen$-N_2-O_2$ in a JSR (1 atm, $\tau = 120$ ms, 1% H_2, $\varphi = 2$, dilution by nitrogen). The data (large symbols) are compared to the modeling (lines).

Figure 4. The oxidation of hydrogen$-N_2-O_2$ in a JSR (10 atm, $\tau = 1000$ ms, 1% H_2, $\varphi = 0.1$, dilution by nitrogen). The data (large symbols) are compared to the modeling (lines).

reactants were diluted by a flow of nitrogen (100 L/h). The fuel and the mixture O_2-N_2 were preheated at a temperature close to that in the reacting JSR zone to reduce temperature gradients in the JSR. The fuel and oxygen flowed separately until they reached the mixing point at the entrance of the injectors. Previous residence time distribution studies showed that this reactor operates under macro-mixing conditions.[11] The JSR operated under steady-state conditions, and, due to the high-dilution of the reactants, no flame occurred. Thus, a perfectly stirred-reactor model could be used. As before,[9−11] a good thermal homogeneity was observed along the vertical axis of the reactor by thermocouple measurements. A Pt/Pt−Rh 10% thermocouple, located inside a thin-wall (<0.5 mm) fused-silica tube to prevent catalytic reactions on the metallic wires of 0.1 mm in diameter, was used. Typical temperature gradients of <10 K were measured. Because a high degree of dilution was used, the temperature rise due to the reaction was generally <30 K. Low pressure samples of the reacting mixtures were taken by sonic probe sampling and collected in 1 L Pyrex bulbs at ca. 50 mbar for immediate gas chromatography (GC) analyses as in refs 5−9. To improve the GC detection, these samples were pressurized at 0.8 bar before injection into the GC column, using a glass homemade piston. Capillary columns of 0.53 mm i.d. × 25 m (Poraplot U and Molecular sieve 5A) were used with a thermal conductivity detector (TCD) and a flame ionization detector (FID) for the measurements of gases, except hydrogen measured on another system. Helium was used as a carrier gas. For hydrogen measurements, a GC operating with nitrogen as carrier gas, a Carboplot (0.53 mm i.d. × 25 m), and a TCD were used. Online Fourier transform infrared (FTIR) analyses of the reacting gases were also performed by connecting the sampling probe to a temperature-controlled (140 °C) gas cell (2 m path length) via a Teflon heated line (130 °C). This analytical system allowed the
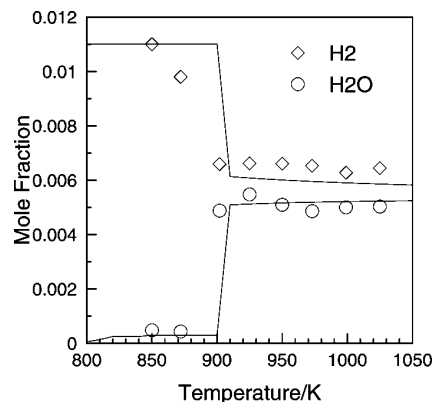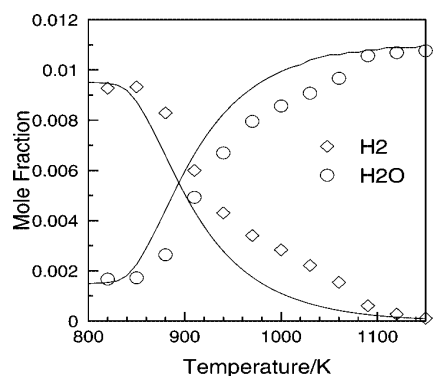
measurements of methane, ethane, ethylene, acetylene, H_2, O_2, H_2O, CO, CH_2O, and CO_2. Very good agreement between the GC and FTIR analyses was found for the compounds measured by both techniques (methane, ethylene, acetylene, CO, CO_2). The reported profiles for hydrocarbons were obtained by GC-FID, and those for CO and CO_2 were measured by FTIR. The reported mole fractions were above the detection limits. Quantitative measurements were limited to 1 ppm for hydrocarbons and 20 ppm for O_2, hydrogen, water, CO, CH_2O, and CO_2. Uncertainties on FTIR measurements were estimated at ca. 10%. Carbon balance was checked for every sample and found good within 100 ± 8% (on average).

3. Kinetic Modeling

The kinetic modeling of premixed flames was performed using the Premix computer code.[12] For simulating the ignition delays, we used the SENKIN code.[13] For the JSR simulations, we used the PSR computer code[14] that computes species concentrations from the balance between the net rate of production of each species by chemical reactions and the

(12) Kee, R. J.; Grcar, J. F.; Smooke, M. D.; Miller, J. A. *Premix: A Fortran program for modeling steady laminar one-dimensional premixed flame*; Sandia National Laboratories: Livermore, CA, 1985; SAND85-8240.

(13) Lutz, A. E.; Kee, R. J.; Miller, J. A. *Senkin: A Fortran program for predicting homogeneous gas phase chemical kinetics with sensitivity analysis*; Sandia National Laboratories: Livermore, CA, 1988; SAND87-8248.

(14) Glarborg, P.; Kee, R. J.; Grcar, J. F.; Miller, J. A. *PSR: A FORTRAN program for modeling well-stirred reactors*; Sandia National Laboratories: Livermore, CA, 1986; SAND86-8209.
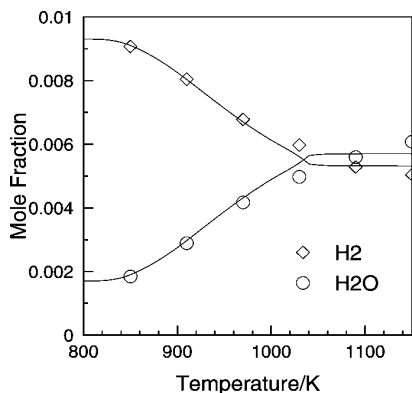
Figure 5. The oxidation of hydrogen$-N_2-O_2$ in a JSR (10 atm, $\tau =$ 1000 ms, 1% H_2, $\varphi = 2.5$, dilution by nitrogen). The data (large symbols) are compared to the modeling (lines).
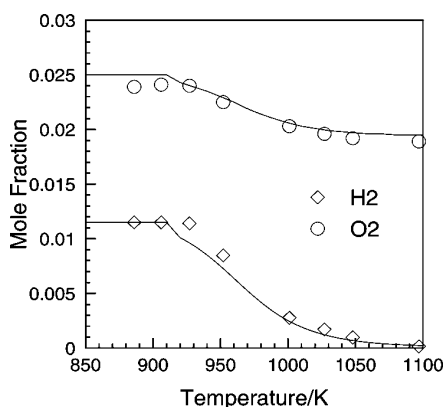

Figure 6. The oxidation of hydrogen$-N_2-O_2$ in a JSR (1 atm, $\tau =$ 120 ms, 1% H_2, $\varphi = 0.2$, dilution by nitrogen, 10% H_2O). The data (large symbols) are compared to the modeling (lines).
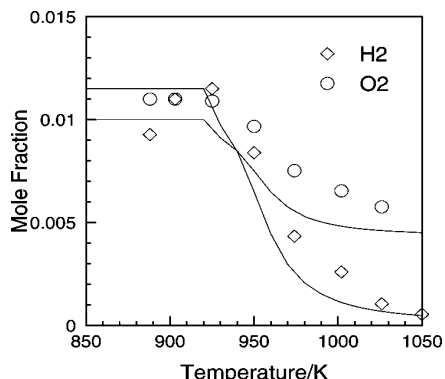

Figure 7. The oxidation of hydrogen$-N_2-O_2$ in a JSR (1 atm, $\tau =$ 120 ms, 1% H_2, $\varphi = 0.5$, dilution by nitrogen, 10% H_2O). The data (large symbols) are compared to the modeling (lines).

difference between the input and output flow rates of species. These rates are computed from the kinetic reaction mechanism and the rate constants of the elementary reactions calculated at the experimental temperature, using the modified Arrhenius equation. The reaction mechanism used here has a strong hierarchical structure. It is based on the comprehensive hydrocarbon oxidation mechanisms[9] developed earlier and recently

Figure 8. The oxidation of hydrogen$-N_2-O_2$ in a JSR (1 atm, $\tau =$ 120 ms, 1% H_2, $\varphi = 1$, dilution by nitrogen, 10% H_2O). The data (large symbols) are compared to the modeling (lines).
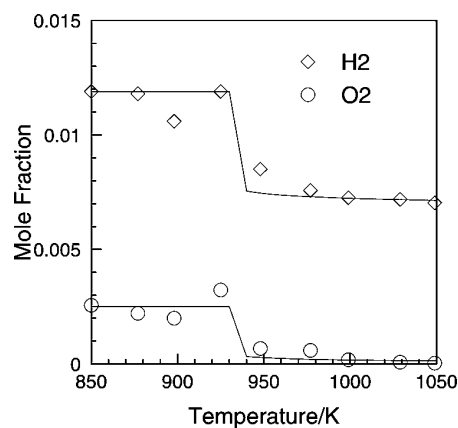
Figure 9. The oxidation of hydrogen$-N_2-O_2$ in a JSR (1 atm, $\tau =$ 120 ms, 1% H_2, $\varphi = 2$, dilution by nitrogen, 10% H_2O). The data (large symbols) are compared to the modeling (lines).

updated.[8,15,16] The reaction mechanism used here consisted of 131 species and 1043 reactions (most of them reversible). The rate constants for reverse reactions are computed from the corresponding forward rate constants and the appropriate equilibrium constants, $K_c = k_{forward}/k_{reverse}$, calculated using thermochemical data.[10,17,18] This mechanism and the corresponding thermochemical data are available from us upon request.

4. Results and Discussion

This study yielded a large set of experimental results for the oxidation of hydrogen- and methane-based fuel mixtures over the temperature range 800−1500 K, for equivalence ratios ranging from 0.1 to 1.5, and for various mole fractions of methane, hydrogen, and water vapor. The experiments were performed at a constant mean residence time of 120 ms at 1 atm. The reaction was studied by varying stepwise

(15) Le Cong, T.; Dagaut, P. Experimental and detailed kinetic modeling of the oxidation of methane and methane/syngas mixtures and effect of carbon dioxide addition. *Combust. Sci. Technol.* **2008**, *180*, 2046–2091.
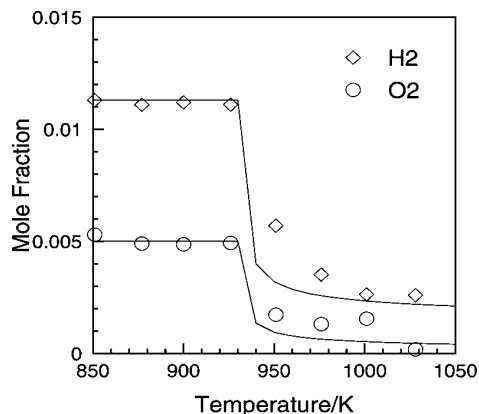
(16) Le Cong, T.; Dagaut, P. Oxidation of H_2/CO_2 mixtures and effect of hydrogen initial concentration on the combustion of CH_4 and CH_4/CO_2 mixtures: Experiments and modeling. *Proc. Combust. Inst.* **2009**, *32*, 2046–2091.

(17) Kee, R. J.; Rupley, F. M.; Miller, J. A. *Thermodynamic Database*; Sandia National Laboratories: Livermore, CA, 1991; SAND87-8215.

(18) Muller, C.; Michel, V.; Scacchi, G.; Côme, G.-M. THERGAS: a computer program for the evaluation of thermochemical data of molecules and free radicals in the gas phase. *J. Chim. Phys. Phys.-Chim. Biol.* **1995**, *92*, 1154–1178.
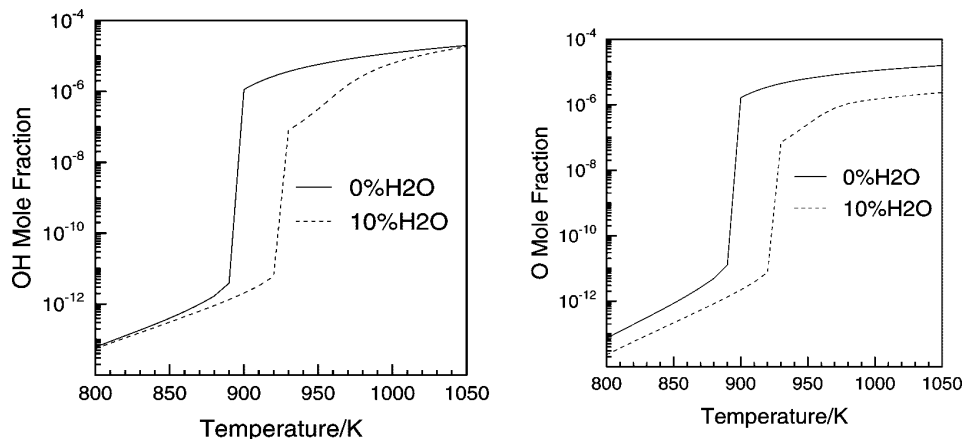
Figure 10. Computed O and OH profiles during the oxidation of $1\%H_2 + O_2 + N_2$ w/o (continuous lines) or with 10% H_2O (dotted lines) at $\varphi = 0.5$ and 1 atm.
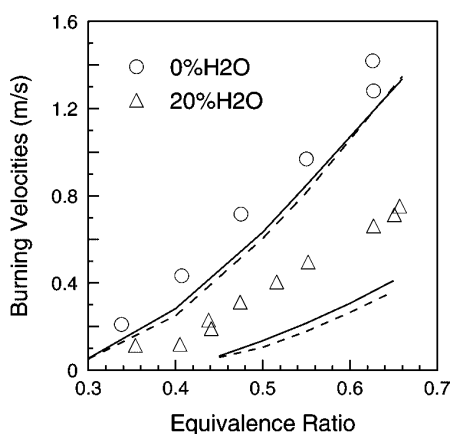

Figure 11. Burning velocities of hydrogen−air flames (353 K, 100 kPa); effect of dilution by water vapor. The data of ref 20 (symbols) are compared to the modeling (this mechanism, continuous lines; GRI 3.0 mechanism, dashed lines).

the operating temperature in the JSR. Concentration profiles for the reactants, stable intermediate compounds, and final products (O_2, H_2, H_2O, CO, CO_2, CH_2O, CH_4, C_2H_6, C_2H_4, and C_2H_2) were obtained. The proposed kinetic reaction mechanism was used to simulate the present experiments.

4.1. Oxidation of Hydrogen−N_2−O_2 and Hydrogen−H_2O−N_2−O_2 Mixtures. The present results allow a comparison of the kinetics of the neat oxidation of hydrogen with that of hydrogen−H_2O mixtures (Figures 1−9). Also, it can be seen that the model represents fairly well this data set for the oxidation of hydrogen. Figures 4 and 5 compare the experimental data obtained at 10 atm by Dagaut and Dayma[19] with our computations, showing a good agreement. At 10 atm, the OH radical is mainly produced by −R18. Reaction paths analyses indicated that increasing the total pressure increases the production of OH via H → HO_2 → H_2O_2 → OH.

The presence of 10% H_2O in mol reduces the rate of oxidation of H_2 through a slower production of radicals. As observed on Figure 10, a shift of the O and OH mole fraction profiles toward higher temperatures was predicted by the model. Hydrogen starts to react at a temperature ca. 50 K

(19) Dagaut, P.; Dayma, G. Hydrogen-enriched natural gas blend oxidation under high pressure conditions: Experimental and detailed chemical kinetic modeling. *Int. J. Hydrogen Energy* **2006**, *31*, 505–515.

higher in the presence of H_2O at $\varphi = 0.5$ and 1 atm. According to our computations, the presence of water vapor favors the reaction:

$$H + O_2 + M = HO_2 + M \qquad (R7)$$
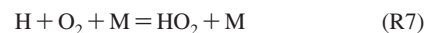
at low temperature due to the higher chaperon efficiency of water (16.25) as compared to that of nitrogen (1.0). This reaction competes with the main branching reaction:

$$H + O_2 = OH + O \qquad (R6)$$

by converting the reactive H atoms into the less reactive HO_2 radicals. The amount of O atoms also decreases in the presence of water vapor through the decreased importance of R6 (Table 1).

PSR computations indicated an increased production of OH radicals via reactions R10 (from 11% to 27% at 1000 K and $\varphi = 0.5$; from 2% to 17% at 1000 K and $\varphi = 2$) and −R18 (from 0% to 20% at 900 K and $\varphi = 0.5$; from 0% to 17% at 900 K at $\varphi = 2$) and a reduction of the OH production via reactions R5 (from 10% to 3.4% at 1000 K and $\varphi = 0.5$; from 30% to 13% at 1000 K and $\varphi = 2$) and R6 (from 24% to 17% at 1000 K and $\varphi = 0.5$; from 27% to 15% at 1000 K and $\varphi = 2$) in the presence of water vapor in the reacting mixture.

$$O + H_2 = OH + H \qquad (R5)$$

Water vapor favors the production of OH by −R18 through the sequence of reactions:

$$H + O_2 + M = HO_2 + M \qquad (R7)$$

$$HO_2 + HO_2 = H_2O_2 + O_2 \qquad (R16)$$

$$H_2O_2 (+M) = OH + OH (+M) \qquad (-R18)$$
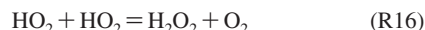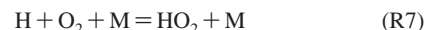
where the high chaperon efficiency of H_2O is a factor. Also, H_2O reacts with O to yield additional OH at high temperature:

$$H_2O + O = OH + OH \qquad (R10)$$

The effect of water−vapor dilution on burning velocities was also studied by simulating experiments taken from the literature (Figure 11) and using the present mechanism and the GRI 3.0 mechanism. The data and the modeling both show the presence of water reduces the burning velocities of hydrogen−air mixtures. However, the kinetic models only qualitatively represent the data that could suffer from underestimated flame stretch and/or overestimation of the amount of water vapor present. Therefore, further data seem necessary to better assess
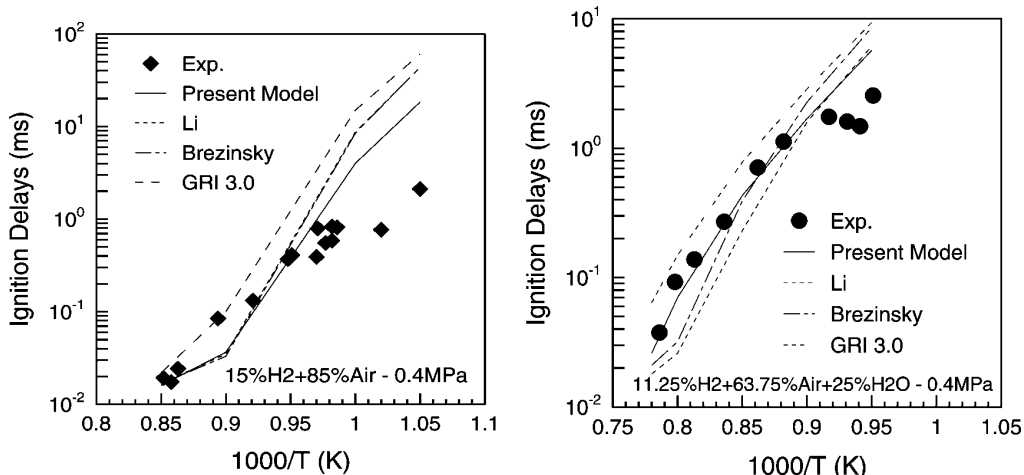
Figure 12. Ignition of hydrogen−air mixtures; effect of dilution by water vapor. The data (symbols) are compared to the modeling (lines).
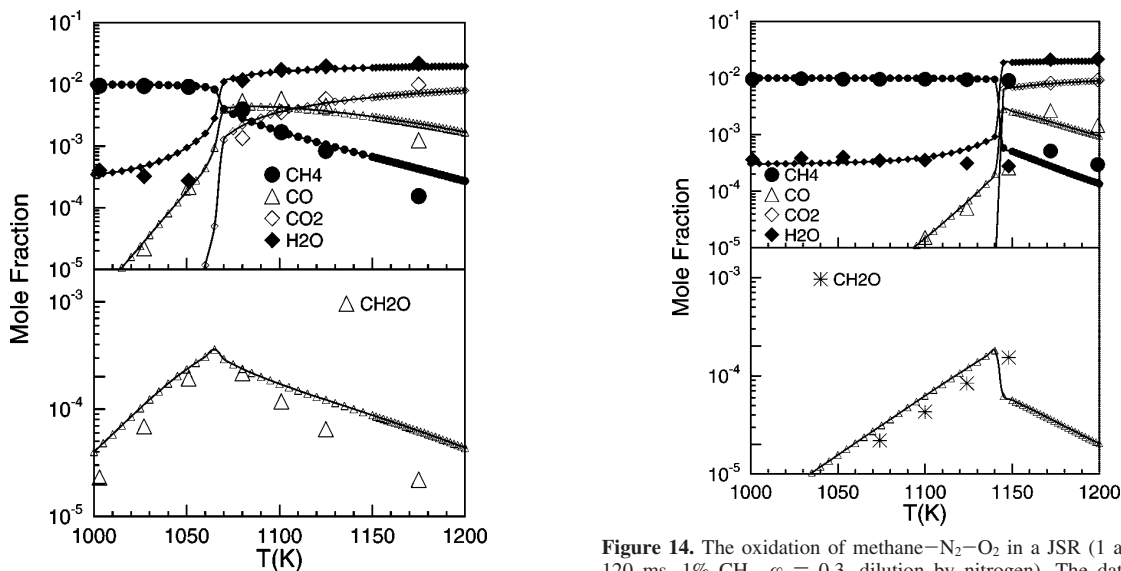

Figure 13. The oxidation of methane−N_2−O_2 in a JSR (1 atm, τ = 120 ms, 1% CH_4, φ = 0.1, dilution by nitrogen). The data (large symbols) are compared to the modeling (lines).

Figure 14. The oxidation of methane−N_2−O_2 in a JSR (1 atm, τ = 120 ms, 1% CH_4, φ = 0.3, dilution by nitrogen). The data (large symbols) are compared to the modeling (lines and small symbols).

the effect of water on hydrogen−air laminar burning velocities. Following our previous work on the effect of burnt gases on fuel combustion,[8] we compared the effect of CO_2 to that of H_2O on burning velocities. This model predicts a stronger reduction of the burning velocities through dilution by CO_2 than by H_2O. This result is essentially due to the increased importance of the reaction CO_2 + H = CO + OH that reduces the concentration of H and consequently reduces the rate of the main branching reaction H + O_2 = OH + O.

Wang et al.[21] have measured the ignition delays of H_2−air−H_2O (ca. 15% H_2 and 0−40% H_2O) over the temperature range 954−1332 K at 1.7 MPa. Figure 12 compares these

data with our computations. Below 1000 K, the model under-predicts the reactivity. This is also the case for models taken from the literature.[22−24] Again, further experimental results obtained below 1000 K would be helpful for further model testing because low-temperature ignition delays that may be subject to large underestimation are currently reconsidered.[25]

4.2. Oxidation of Methane−N_2−O_2 and Methane−H_2O−N_2−O_2 Mixtures. A second set of experiments was performed for the oxidation of methane and methane−water vapor mixtures in a JSR. The examination of the present results allows a comparison of the kinetics of oxidation of methane and methane−water vapor mixtures (Figures 13−17).

The computations showed that in fuel-lean conditions, CH_4 oxidation yields more CH_2O than C_2H_6, whereas the route to C_2 hydrocarbons is favored in fuel-rich conditions. At high

(20) Lamoureux, N.; Djebaili-Chaumeix, N.; Paillard, C. E. Laminar flame velocity determination for H_2-air-steam mixtures using the spherical bomb method. *J. Phys. (Paris)* **2002**, *12*, 445–452.

(21) Wang, B. L.; Olivier, H.; Grönig, H. Ignition of shock-heated H_2-air-steam mixtures. *Combust. Flame* **2003**, *133*, 93–106.

(22) Smith, G. P.; Golden, D. M.; Frenklach, M.; Moriarty, N. W.; Eiteneer, B.; Goldenberg, M.; Bowman, C. T.; Hanson, R. K.; Song, S.; Gardiner, W. C., Jr.; Lissianski, V. V.; Qin, Z. 1999, available on: http://www.me.berkeley.edu/gri_mech/.

(23) Li, J.; Zhao, Z.; Kazakov, A.; Dryer, F. An updated comprehensive kinetic model of hydrogen combustion. *Int. J. Chem. Kinet.* **2004**, *36*, 566–575.

(24) Sivaramakrishnan, R.; Comandini, A.; Tranter, R. S.; Brezinsky, K.; Davis, S. G.; Wang, H. Combustion of CO/H_2 mixtures at elevated pressures. *Proc. Combust. Inst.* **2007**, *31*, 429–437.

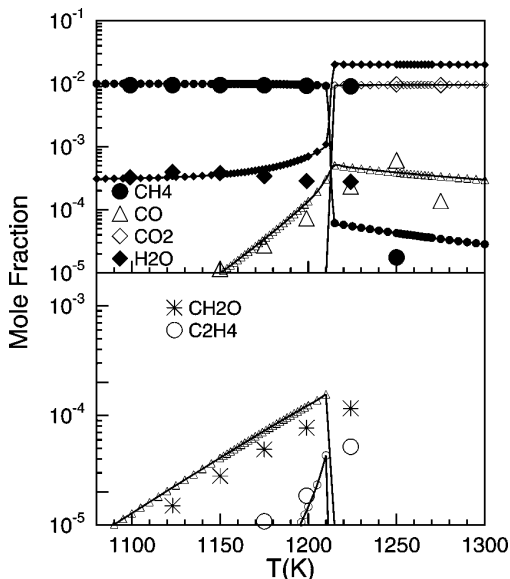(25) Petersen, E. 2008, private communication.

Figure 15. The oxidation of methane$-N_2-O_2$ in a JSR (1 atm, $\tau =$ 120 ms, 1% CH_4, 1 $\varphi = 0.6$, dilution by nitrogen). The data (large symbols) are compared to the modeling (lines and small symbols).
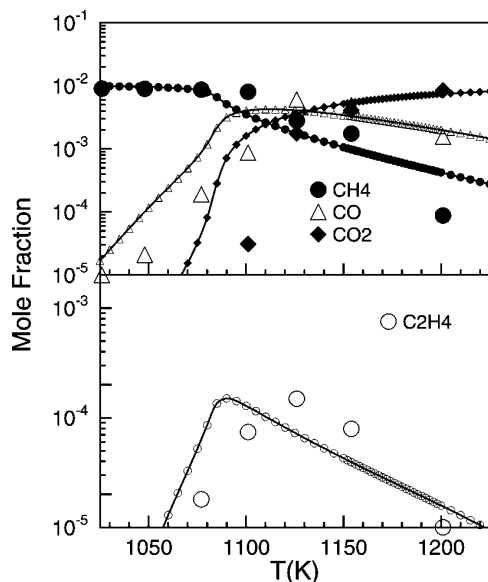

Figure 16. The oxidation of methane$-N_2-O_2$ in a JSR (1 atm, $\tau =$ 120 ms, 1% CH_4, 10% H_2O, $\varphi = 0.1$, dilution by nitrogen). The data (large symbols) are compared to the modeling (lines and small symbols).

pressure and low temperature, the recombination reactions are important. Increasing the total pressure increases the importance of the channels $CH_3 + H$ and $CH_3 + CH_3$. Methane is mostly consumed by reaction with OH:

$$CH_4 + OH = CH_3 + H_2O \qquad (R77)$$

When the equivalence ratio increases, methane reaction with H is becoming more important:

$$CH_4 + H = CH_3 + H_2 \qquad (R79)$$

The present measurements indicate that the presence of 10% H_2O tends to inhibit the oxidation of methane. Reaction path analyses were performed to interpret the results in the following
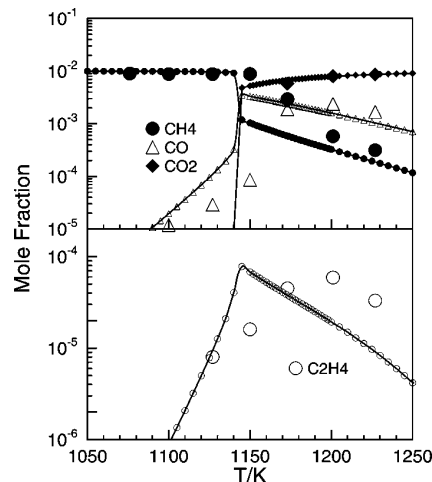

Figure 17. The oxidation of methane$-N_2-O_2$ in a JSR (1 atm, $\tau =$ 120 ms, 1% CH_4, 10% H_2O, $\varphi = 0.3$, dilution by nitrogen). The data (large symbols) are compared to the modeling (lines and small symbols).

conditions: 1% $CH_4-O_2-N_2$ and 1% $CH_4-10\%$ $H_2O-O_2-N_2$ at $\varphi = 0.3$, 1 atm, $\tau = 120$ ms, and $T = 1140$ K (Figure 18). The analyses indicated that water participates in the reaction:

$$H_2O + O = OH + OH \qquad (R10)$$

This reaction consumes O-atoms (20%) and yields OH (6%). In the absence of water, O-atoms significantly react with methane (80%). In the presence of 10% water, the importance of this channel is strongly reduced because it represents only 60%.

$$CH_4 + O = CH_3 + OH \qquad (R78)$$
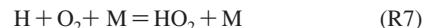
The consumption of H through reaction R6:

$$H + O_2 = OH + O \qquad (R6)$$

decreases (45% in the absence of water and 38% in the presence of water), whereas it increases via R7 (H + O_2 + M = HO_2 + M): 10% in the absence of water and 22% in the presence of water. Here, the third body efficiency of water, significantly higher than that of nitrogen, is a factor (Figure 19).

The chemical effect of H_2O yields a reduction of the concentration of the main radicals responsible for methane consumption (Figure 18). Furthermore, the competition between reactions R10 and R78,

$$H_2O + O = 2OH \qquad (R10)$$

$$CH_4 + O = CH_3 + OH \qquad (R78)$$

and that between reactions R7 and R79,

$$H + O_2 + M = HO_2 + M \qquad (R7)$$

$$CH_4 + H = CH_3 + H_2 \qquad (R79)$$

yield a slower consumption of CH_4 in the presence of water. Therefore, these computations and the present experimental results demonstrate that water vapor inhibits the oxidation of methane under the present JSR conditions.

Gurentsov et al.[26] have measured the ignition delays of methane mixtures in the presence of H_2O in a shock-tube. We

(26) Gurentsov, E. V.; Divakov, O. G.; Eremin, A. V. Ignition of multicomponent hydrocarbon/air mixtures behind shock waves. *High Temp.* **2002**, *40*, 379–386.
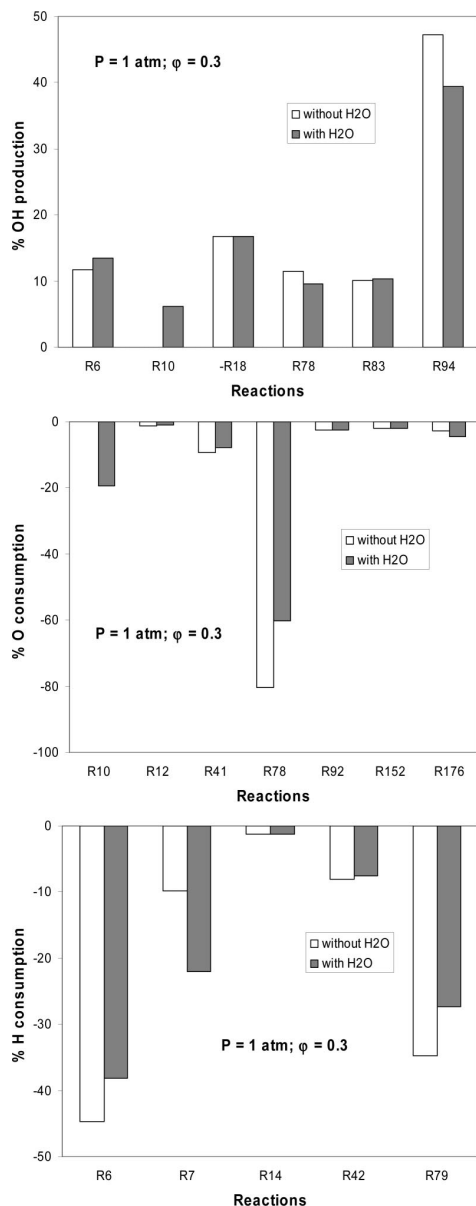
Figure 18. Reaction paths for OH, O, and H during the oxidation of $CH_4-N_2-O_2$ and $CH_4-H_2O-N_2-O_2$ in a JSR (1 atm, 1140 K, $\tau =$ 120 ms, 1% CH_4, 0 or 10% H_2O, $\varphi = 0.3$).

have simulated these experiments to further investigate the effect of water vapor on the kinetics of methane oxidation. Two mixtures were considered: 9.5% $CH_4-19\%$ $O_2-71.5\%$ Ar and 8% $CH_4-8\%$ $H_2O-17\%$ $O_2-67\%$ Ar, in the pressure range 3.3−7.6 atm and temperatures ranging from 1455 to 1885 K. The present model predicts reasonably well the increase of ignition delays in the presence of water, as can be seen from Figure 20. The modeling also indicated a decreased reactivity of the mixture in the presence of water results from the same reaction paths delineated under JSR conditions.

Suh and Atreya[27] and Atreya et al.[28] have studied the effect of water vapor in a methane−air diffusion flame (keeping constant the concentration of O_2 at 20% and the ratio CH_4/N_2 at 75%/25% on the fuel side).

Figure 19. Computed reaction rate during the oxidation of methane$-N_2-O_2$ and methane$-H_2O-N_2-O_2$ in a JSR (1 atm, 1140 K, $\tau =$ 120 ms, 1% CH_4, 0 or 10% H_2O, $\varphi = 0.3$, dilution by nitrogen).
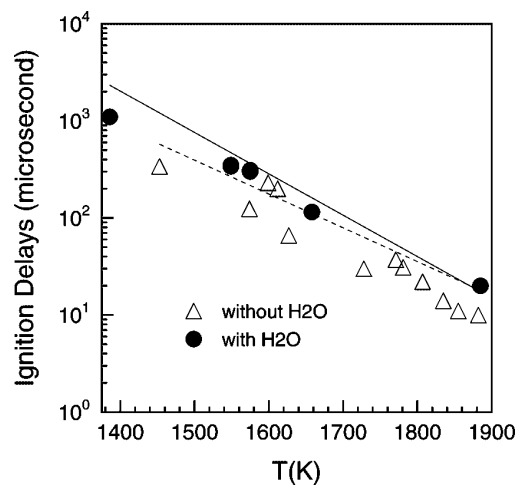
Figure 20. Ignition of methane$-O_2-$Ar and methane$-O_2-$Ar$-H_2O$ mixtures; effect of dilution by water vapor. The data (symbols) are compared to the modeling (lines). Mixtures: 9.5% $CH_4-19\%$ $O_2-71.5\%$ Ar and 8% $CH_4-8\%$ $H_2O-17\%$ $O_2-67\%$ Ar; $P = 3.3-7.6$ atm; $T = 1455-1885$ K from ref 26.

The authors have shown the maximum flame temperature and the concentration of CO_2 increase with the increased concentration of water, whereas the concentration of CO decreases as a result of the increased concentration of OH that oxidizes CO into CO_2.

Renard et al.[29] have measured the structure of a $C_2H_2-O_2-$Ar flame and studied the effect of H_2O on the formation of intermediates. Their results showed that water influences the flame chemistry via the production of OH through $H_2O + H = OH + H_2$, responsible for the reduced concentration of intermediate hydrocarbons in the flame.

(27) Suh, J.; Atreya, A. The effect of water vapor on counterflow diffusion flames. *Proceedings of 3rd International Conference on Fire Research and Engineering*; Orlando, 1995; pp 103−108.
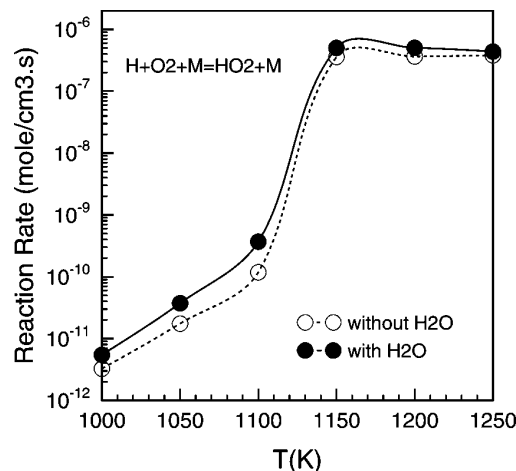
(28) Atreya, A.; Crompton, T.; Suh, J. A study of the chemical and physical mechanisms of fire suppression by water. *Proceedings of 7th International Conference on Fire Research and Engineering*; Poitiers, France, 1999; pp 493−504.

(29) Renard, C.; Musick, M.; Van Tiggelen, P. J.; Vandooren, J. Effect of CO_2 or H_2O addition on hydrocarbon intermediates in rich $C_2H_4/O_2/$Ar flames. *Proc. European Combustion Meeting*; Orléans, France, October 25−28, 2003.
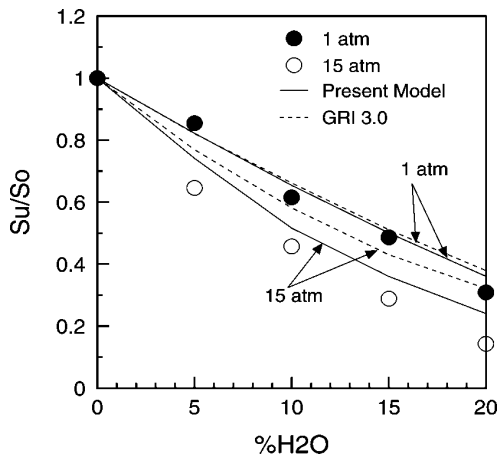
Figure 21. Effect of H_2O on the burning velocities of stoichiometric CH_4–air mixtures at 200 °C. The data of ref 32, symbols, are compared to the modeling (lines).
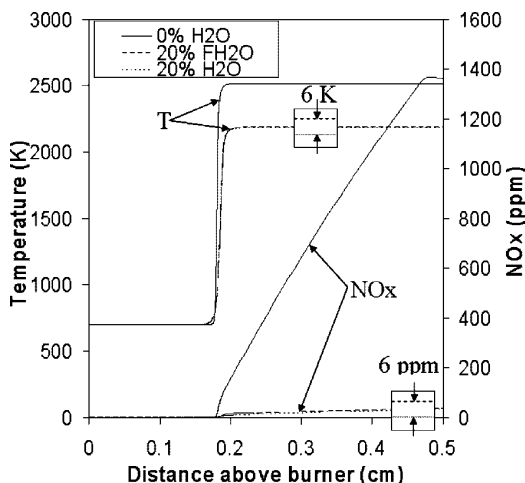

Figure 22. Effect of 20% H_2O (substitution) on the flame temperatures and NO_x emission of stoichiometric CH_4–air mixtures at $T_o = 700$ K, $P = 20$ atm.

Figure 23. Effect of 20% H_2O (substitution) on the flame temperatures and NO_x emission of stoichiometric CH_4–CO–H_2–air mixtures at $T_o = 700$ K, $P = 20$ atm.

Figure 24. Effect of H_2O on the concentration of NO_x emission in stoichiometric CH_4–air flame at $T_o = 700$ K, $P = 20$ atm. Computed results with increasing substitution of N_2 by H_2O.

Hwang et al.[30] simulations of CH_4–O_2–N_2 diffusion flames have shown the reaction $H_2O + O = OH + OH$ is mostly responsible for the chemical effect of H_2O. Thermal effects are also important in flames. Several studies have demonstrated that water reduces the burning velocity of hydrocarbons.[31-33] Figure 21 shows the present model predicts well the reduced burning velocities of methane–air laminar flames at 1 and 15 atm in the presence of H_2O.

4.3. Effect of H_2O on NO_x Formation under Gas Turbine Conditions. The emission of NO_x from gas turbines operating under high pressure and high temperature can be controlled via H_2O injection. However, it is unclear how the
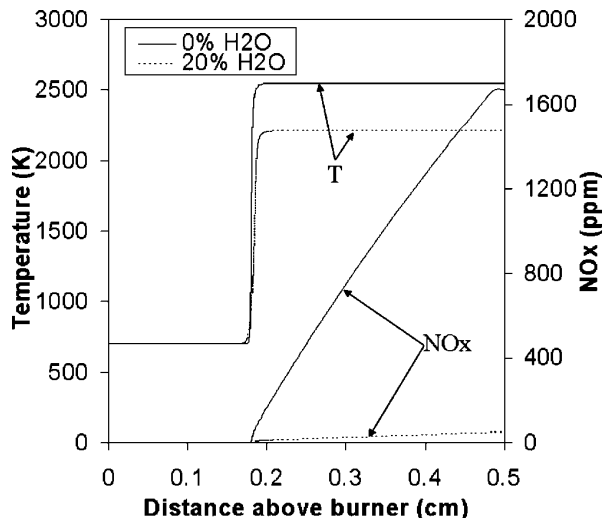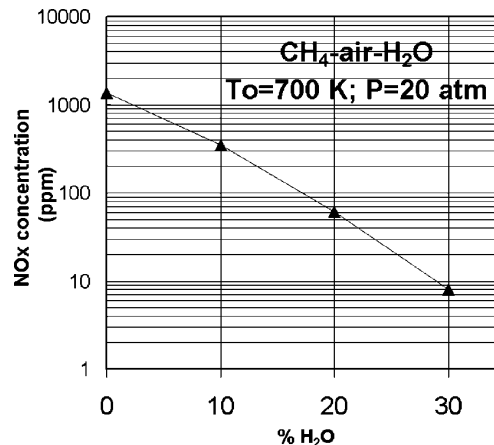
reduction of NO_x emission proceeds. Therefore, we have investigated numerically the formation of NO_x in various conditions using the NO_x subscheme of ref 34. Two stoichiometric flames, CH_4–air and CH_4–CO–H_2–air (50% CH_4–25% CO–25% H_2) without and with 10%, 20%, and 30% in volume of water (substituting N_2 by H_2O), were considered first. The initial conditions were chosen close to those of gas turbine operation: $T_o = 700$ K and $P = 20$ atm.

The computed results are presented in Figures 22–24 showing a strong reduction of NO by increasing the initial concentration of water vapor. Also, Figures 22 and 23 clearly show the adiabatic flame temperature is reduced by ca. 200 K in the presence of 20% vol of water vapor. The use of a fake water species in the modeling allowed us to evaluate the relative importance of the chemical and physical effect of water on NO_x formation and flame temperature. If the fake H_2O has the physical properties of H_2O (thermochemistry and transport) but does not react in the chemical scheme (Figure 22), most of the

(30) Hwang, D.-J.; Choi, J.-W.; Park, J.; Keel, S.-I.; Ch, C.-B.; Noh, D.-S. Numerical study on flame structure and NO formation in CH_4–O_2–N_2 counterflow diffusion flame diluted with H_2O. *Int. J. Energy Res.* **2004**, *28*, 1255–1267.

(31) Fells, I.; Rutherford, A. G. Burning velocity of methane-air flames. *Combust. Flame* **1969**, *13*, 130–138.

(32) Babkin, V. S.; V'yun, A. V. Effect of water vapor on the normal burning velocity of a methane-air mixture at high pressures. *Combust., Explos. Shock Waves* **1971**, *7*, 339–341.

(33) Müller-Dethlefs, K.; Schlader, A. F. The effect of steam on flame temperature, burning velocity and carbon formation in hydrocarbon flames. *Combust. Flame* **1976**, *27*, 205–215.

(34) Dagaut, P.; Glarborg, P.; Alzueta, M. U. The oxidation of hydrogen cyanide and related chemistry. *Prog. Energy Combust. Sci.* **2008**, *34*, 1–46.
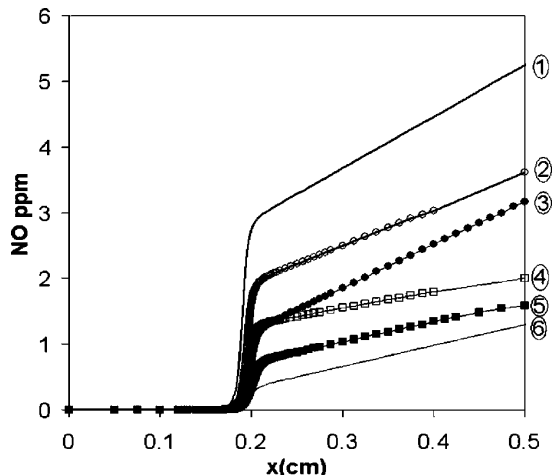
Figure 25. Effect of 20% N_2 replaced by H_2O on the NO_x emission of CH_4−air mixtures ($\varphi = 0.5$) at $T_o = 700$ K, $P = 20$ atm. Line 1: CH_4−air. Line 2: CH_4−O_2−N_2−20% FH_2O (Cp and ε of N_2). Line 3: CH_4−O_2−N_2−20% FH_2O (Cp of N_2 and ε of H_2O). Line 4: CH_4−O_2−N_2−20% FH_2O (Cp of H_2O and ε of N_2). Line 5: CH_4−O_2−N_2−20% FH_2O (Cp and ε of H_2O). Line 6: CH_4−O_2−N_2−20% H_2O.
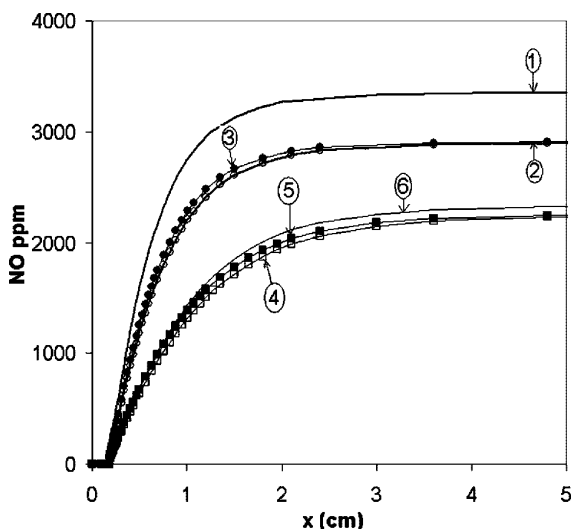

Figure 26. Effect of 20% N_2 replaced by H_2O on the NO_x emission of CH_4−air mixtures ($\varphi = 1$) at $T_o = 700$ K, $P = 20$ atm. Line 1: CH_4−air. Line 2: CH_4−O_2−N_2−20% FH_2O (Cp and ε of N_2). Line 3: CH_4−O_2−N_2−20% FH_2O (Cp of N_2 and ε of H_2O). Line 4: CH_4−O_2−N_2−20% FH_2O (Cp of H_2O and ε of N_2). Line 5: CH_4−O_2−N_2−20% FH_2O (Cp and ε of H_2O). Line 6: CH_4−O_2−N_2−20% H_2O.

effect of H_2O on flame temperature and NO_x formation is not due to the kinetics but to thermal effects.

For a more detailed evaluation of the chemical and thermal effect of water, we have changed the thermochemistry properties of the fake water compound. The use of the thermochemical properties of N_2 for this fake water allowed eliminating the thermal effect. Also, the third body coefficients (ε) of H_2O in the elementary reactions (16.25) were replaced by that of N_2 (1.0), allowing one to quantify the water third body effect on the formation of NO_x. The computed results are showed in Figures 25−27 for mixtures CH_4−air in lean and stoichiometric conditions ($\varphi = 0.5$ and $\varphi = 1$). As can be seen from Figures 25 and 26, the global reduction of NO_x by replacement of 20% N_2 by H_2O is
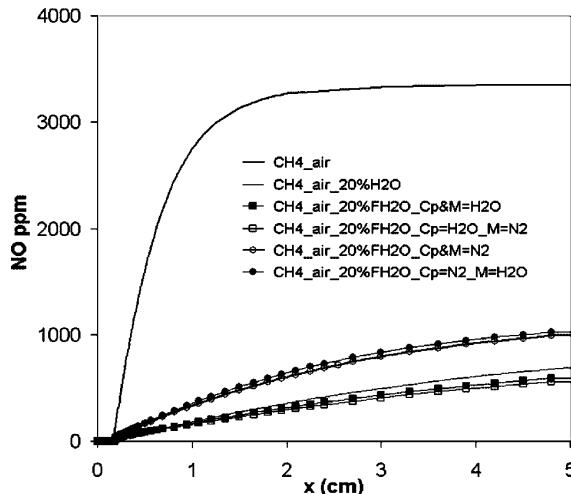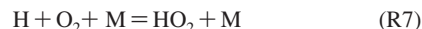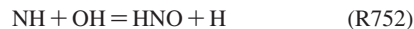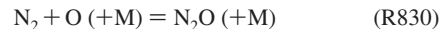

Figure 27. Effect of 20% H_2O on the NO_x emission of stoichiometric CH_4−air mixtures at $T_o = 700$ K, $P = 20$ atm. The thick solid line refers to the methane−air case (top of the figure), and the solid line refers to the methane−air−H_2O (20%) case. The other lines represent the simulations performed using fake H_2O (■, methane−air−fake-H_2O (20%) with Cp of H_2O and chaperon efficiency of H_2O; □, methane−air−fake-H_2O (20%) with Cp of H_2O and chaperon efficiency of N_2, that is, equal to 1;○, methane−air−fake-H_2O (20%) with Cp of N_2 and chaperon efficiency of N_2; ●, methane−air−fake-H_2O (20%) with Cp of N_2 and chaperon efficiency of H_2O).

observed between line 1 and line 6. The variation from line 1 to line 2 is due to the reduction of N_2 initial concentration by water vapor substitution. The variation from line 3 to line 5 is due to the thermal effect. The variation from line 5 to line 6 is due to the chemical effect. The variations from line 2 to line 3 and from line 4 to line 5 are due to the third body effect.

It is clearly shown that the chemical effect of water on the formation of NO_x in fuel-lean conditions is higher than that in stoichiometric conditions. In fact, under fuel-lean conditions, the concentrations of O_2 and O radical are higher than in stoichiometric mixtures. There, water vapor reduces the formation of NO_x by reducing the formation of oxygen radical, the main agent of NO_x production. The impact of water on oxygen radical proceeds through the reactions:

$$H + O_2 + M = HO_2 + M \qquad \text{(R7)}$$

$$H_2O + O = 2OH \qquad \text{(R10)}$$

whereas NO is produced via:

$$N_2 + O = NO + N \qquad \text{(R749)}$$

$$N + O_2 = NO + O \qquad \text{(R826)}$$

$$N_2 + O \,(+M) = N_2O \,(+M) \qquad \text{(R830)}$$

$$N_2O + OH = NH + N_2O \qquad \text{(R761)}$$

$$NH + OH = HNO + H \qquad \text{(R752)}$$

$$HNO + O = NO + OH \qquad \text{(R817)}$$

$$HNO + OH = NO + H_2O \qquad \text{(R818)}$$

$$HNO + H = NO + H_2 \qquad \text{(R819)}$$

In stoichiometric mixtures (Figure 26), the chemical effect of water on the final concentration of NO_x is reversed. In other words, water vapor enhances the formation of NO_x in

**Table 1. Important Reactions from the Reaction Mechanism Used in This Study**[a]

reaction	A	n	E
5. $O + H_2 = OH + H$	1.30×10^{04}	2.8	5922.0
6. $H + O_2 = OH + O$	1.90×10^{14}	0.0	16 812.0
7. $H + O_2 + M = HO_2 + M$	8.00×10^{17}	−0.8	0.0
10. $H_2O + O = OH + OH$	1.50×10^{10}	1.1	17 260.0
12. $HO_2 + O = OH + O_2$	2.44×10^{13}	0.0	−446.0
14. $H + HO_2 = OH + OH$	8.40×10^{13}	0.0	874.0
16. $HO_2 + HO_2 = H_2O_2 + O_2$	4.20×10^{14}	0.0	11 982.0
17. $HO_2 + HO_2 = H_2O_2 + O_2$	1.30×10^{11}	0.0	−1630.0
18. $+OH (+M) = H_2O_2 (+M)$	7.40×10^{13}	−0.4	0.0
k_0:	0.23×10^{19}	−0.90	−1700.0
Troe centering:	0.7346; 94; 1756; 5182		
41. $CH_2O + O = HCO + OH$	1.81×10^{13}	0.0	3088.0
42. $CH_2O + H = HCO + H_2$	1.10×10^{08}	1.8	3000.0
77. $CH_4 + OH = CH_3 + H_2O$	2.60×10^{06}	2.1	2462.0
78. $CH_4 + O = CH_3 + OH$	1.62×10^{06}	2.3	7094.0
79. $CH_4 + H = CH_3 + H_2$	2.25×10^{04}	3.0	8756.6
83. $CH_3 + HO_2 = CH_3O + OH$	5.00×10^{12}	0.0	0.0
94. $CH_3 + O_2 = CH_2O + OH$	6.62×10^{11}	0.0	14 188.0
152. $C_2H_6 + O = C_2H_5 + OH$	9.99×10^{08}	1.5	5803.0
176. $C_2H_4 + O = CH_2HCO + H$	1.50×10^{07}	1.9	184.0
749. $N_2 + O = N + NO$	1.00×10^{14}	0.0	75 490.0
752. $NH + OH = HNO + H$	2.00×10^{13}	0.0	0.0
761. $NH + NO_2 = N_2O + OH$	1.00×10^{13}	0.0	0.0
804. $NO + OH (+M) = HONO (+M)$	1.99×10^{12}	−0.1	−721.0
k_0:	5.08×10^{23}	−2.5	−67.6
Troe centering:	0.620; 10; 100 000.0		
813. $HONO + OH = NO_2 + H_2O$	1.30×10^{10}	1.0	135.0
817. $HNO + O = NO + OH$	1.00×10^{13}	0.0	0.0
818. $HNO + OH = NO + H_2O$	3.60×10^{13}	0.0	0.0
819. $HNO + H = NO + H_2$	4.40×10^{11}	0.7	650.0
826. $N + O_2 = NO + O$	6.40×10^{09}	1.0	6280.0
830. $N_2O (+M) = N_2 + O (+M)$	1.30×10^{12}	0.0	62 570.0

[a] Note $k = A \times T^n \times \exp(−E/1.9872 \times T)$ given at 10 atm. Units: mole, cm^3, s, K, cal, mole.

stoichiometric conditions. Reaction path analyses showed that the main reaction producing NO at 5 cm from the burner is:

$$HONO + (M) = NO + OH (+M) \quad (R804)$$

HONO is formed via:

$$NO_2 + H_2O = HONO + OH \quad (R813)$$
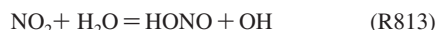
In the case where H_2O dilution is used (Figure 27), the effect of water on NO production is strong. However, as shown in Figure 27, the chemical effect in this case can be considered negligible.

5. Conclusion

New experiments were performed for the oxidation of hydrogen-based and methane-based fuels (H_2, CH_4, H_2/H_2O, CH_4/H_2O) in a fused silica jet-stirred reactor (JSR) operating at 1−10 atm, over the temperature range 800−1300 K, from fuel-lean to fuel-rich conditions. The detailed chemical kinetic modeling of these experiments was performed yielding generally a good agreement with the present data and experimental results taken from the literature (burning velocities and ignition delays). Reaction paths analyses were used to delineate the important reactions influencing the kinetic of oxidation of the fuels in presence of water vapor. The kinetic modeling indicates the inhibition by water vapor addition under JSR conditions is mainly due to the high third body efficiency of H_2O to remove H in $H + O_2 + M = HO_2 + M$ and to the reaction $H_2O + O = 2OH$, competing with the oxidation of methane via $CH_4 + O = CH_3 + OH$. In premixed flames, the increased concentration of H_2O yields lower flame speeds, lower adiabatic temperature, and reduced NO_x formation. Kinetic analyses indicated that the reduction of NO emission by H_2O injection is mostly due to dilution, reduction of N_2 concentration, and thermal effects.